Binding Synergy and Cooperativity in Dihydrodipicolinate Reductase: Implications for Mechanism and the Design of Biligand Inhibitors[†]

Xia Ge, Andrew Olson, Sheng Cai, and Daniel S. Sem*

Chemical Proteomics Facility at Marquette, Department of Chemistry, P.O. Box 1881, Marquette University, Milwaukee, Wisconsin 53201

Received April 21, 2008; Revised Manuscript Received July 21, 2008

ABSTRACT: Dihydrodipicolinate reductase (DHPR) is a homotetramer that catalyzes reduction of dihydrodipicolinate (DHP). We recently reported a biligand inhibitor (K_i = 100 nM) of DHPR, comprised of fragments that bind in the NADH (CRAA = catechol rhodanine acetic acid) and DHP (PDC = pyridine dicarboxylate) binding sites. Herein, we characterize binding synergy and cooperativity for ligand binding to *Escherichia coli* DHPR: NADH or CRAA and PDC (stable analog of DHP). While K_d values indicate little synergy between NADH and PDC, ^{1}H-^{15}N HSQC chemical shift perturbation and saturation transfer difference (STD) titrations indicate that PDC induces a more dramatic conformational change than NADH, consistent with a role in domain closure. PDC binds cooperatively (Hill coefficient = 2), while NADH does not, based on STD titrations that monitor only fast exchange processes. However, HSQC titrations monitoring Trp253 (located between monomers) indicate that NADH binds in two steps, with high affinity binding to only one of the monomers. Therefore, DHPR binds cofactor via a sequential model, with negative cooperativity. These results, interpreted in light of steady-state data, suggest that DHPR activity requires NADH binding at only one of the four monomers. Implications of our results for fragment assembly are discussed, using CRAA tethering to PDC as a model biligand: (a) if one fragment (ex. PDC) must induce a large structural change before the other fragment is brought proximal, this must be screened for upfront, and (b) cooperative or synergistic interactions between binding sites can lead to unexpected and misleading effects in NMR-based screening.

INTRODUCTION

Dihydrodipicolinate reductase (DHPR)[1] catalyzes the pyridine nucleotide-dependent reduction of dihydrodipicolinic acid to form tetrahydrodipicolinic acid (Figure 1a). It is part of the biosynthetic pathway leading to *meso*-diaminopimelic acid and L-lysine in bacteria and higher plants, and is therefore a potential target for new antimicrobial and herbicidal compounds (*1, 2*). *Escherichia coli* (*E. coli*) and *Mycobacterium tuberculosis* (*Mtb*) DHPR X-ray crystal structures have been reported for various complexes (*3*−*5*). DHPR has a cofactor binding site in an N-terminal Rossmann-fold domain and a substrate binding site in its C-terminal domain, which also serves as a core for forming the active homotetramer. The two domains are connected via flexible hinge regions. The NMR binding studies presented herein are directed to exploring interactions of DHPR's two substrate binding sites (i.e., synergy), as well as interactions between the 4 monomers that comprise the active tetramer (i.e., cooperativity). Such information is required to better define the mechanism, and should also facilitate rational drug design targeting adjacent DHPR binding sites. Protein−ligand interactions and binding synergy have important implications for fragment-based drug assembly when multiple binding sites are targeted. Fragment assembly strategies must address the challenge of how to build inhibitors that consider binding synergy, rather than considering only static structures with noninteracting binding sites.

Although DHPR exists as a tetramer in its native state, crystal structures of the ternary complex contain only three molecules of cofactor NADH and substrate analog 2,6-pyridine dicarboxylate (PDC). The structure indicates that the three monomers of DHPR are in a closed form, with the remaining monomer in an unbound and open conformation (*5*). Why and by what mechanism this occurs is not known. DHPR appears to bind both NADH and NADPH with similar affinity, and ITC (isothermal titration calorimetry) titrations indicate that there is a one to one stoichiometry for cofactor and enzyme binding (*6*), which contrasts with the crystallography data that indicate 3 out of 4 sites are occupied.

[†] This research was supported, in part, by Marquette University and by the National Institutes of Health/National Science Foundation Instrumentation Grants 510 RR019012 and CHE-0521323, and an NIH-NCRR-SEPA funded outreach program grant (R25-RR022749).

* Address correspondence to this author: (414) 288-7859 (phone), (414) 288-7066 (fax), Daniel.Sem@marquette.edu (email).

[1] Abbreviations: CRAA, catechol rhodanine acetic acid; DHP, dihydrodipicolinate; DHPR, dihydrodipicolinate reductase; DHPS, dihydrodipicolinate synthase; DTT, dithiothreitol; HSQC, heteronuclear single quantum coherence; IPTG, isopropyl α-D-1-thiogalactopyranoside; KNF, Koshland, Nemethy, and Filmor; Mtb, *Mycobacterium tuberculosis*; MWC, Monod, Wyman, and Changeux; NADH, nicotinamide adenine dinucleotide (reduced); NAD^+, nicotinamide adenine dinucleotide (oxidized); NMR, nuclear magnetic resonance; NOE, nuclear Overhauser effect; PDC, pyridine 2,6-dicarbxylate; SDS-PAGE, sodium dodecylsulfate-polyacrylamide gel electrophoresis; STD, saturation transfer difference; THP, tetrahydrodipicolinate; TROSY, transverse relaxation optimized spectroscopy.

10.1021/bi8007005 CCC: $40.75
Published on Web 08/19/2008

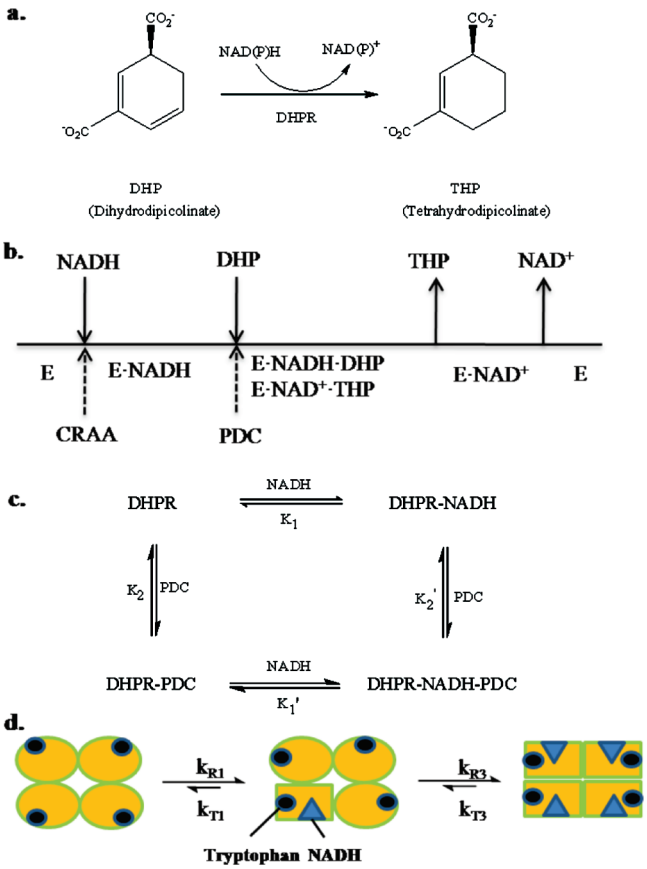

FIGURE 1: (a) *E. coli* DHPR catalyzed reduction of dihydrodipicolinate (DHP) to tetrahydrodipicolinate (THP). (b) Schematic representation of the kinetic mechanism of *E. coli* dihydrodipicolinate reductase (DHPR) with inhibition by 1,6-pyridine dicarboxylate (PDC) and CRAA. The DHPR reaction goes by an ordered sequential mechanism in which the binding of NADH is followed by dihydrodipicolinate binding and with tetrahydrodipicolinate release preceding NAD^+ release (*6*). Such a mechanism suggests DHP (and PDC) bind tighter to E•NADH than to apo DHPR. (c) ligand binding in the two sequences explored in this paper, to define the binding synergy observed in the steady-state. This binding scheme is a simplification, because the DHPR tetramer actually contains four cofactor NADH binding sites and four substrate (DHP or PDC) binding sites that may show cooperativity. (d) Cartoon rendering of the DHPR tetramer binding to cofactor NADH. The NMR reporter residue used in this study, Trp253, is located in a sensitive loop region between monomers, which is packed against the Rossmann domain.

Adding to the uncertainty about binding site cooperativity and interactions, Kefala (*7*) et al. reported another three X-ray crystal structures for *Mtb* DHPR, and claimed that different structures were resulting from different crystallization conditions. While X-ray crystal structures provide only static snapshots of protein structure, they provide a solid foundation for complementary methods, such as NMR spectroscopy, to build upon and further define domain interactions and interconversions between states, which is the topic of this paper.

Besides helping to describe an enzyme's mechanism, studies of binding site interactions can aid in subsequent structure based drug design efforts, such as fragment assembly methods that target adjacent binding pockets. Fragment-based drug discovery is widely used as a method for drug-lead identification (*8*−*11*); it capitalizes on the modular binding of low molecular weight and low-affinity ligands, which become high affinity when chemically linked. However, the deconstruction of potent enzyme inhibitors into their respective fragments reveals that there can be surprising complexity in dealing with low-affinity ligands (*8, 12*), especially when they occupy synergistically interacting binding sites. In this regard, we have recently reported fragment assembly efforts with DHPR, whereby a catechol-rhodanine acetic acid (CRAA) ligand that binds in the NADH pocket was tethered to 2,6-pyridine dicarboxylate (PDC), a stable analog of the DHP (dihydrodipicolinate) substrate. One troubling result of that study was the fact that CRAA inhibition, which was competitive vs NADPH, occurred with a Hill coefficient of 2 (*13*). This led to questions as to what role binding site synergy or cooperativity has in DHPR mechanism, and how this might impact fragment assembly efforts. Furthermore, since crystal structures indicate that all four DHPR monomers are not identical, in terms of their ability to bind substrates, there may be cooperativity between the monomers.

The above-mentioned studies of *E. coli* DHPR indicate the importance of considering binding synergy, cooperativity and dynamics in mechanism, with implications for fragment assembly for flexible protein targets with potentially interacting sites. As a complementary method to X-ray crystallography, NMR could help define these interactions and corresponding structural changes for complexes that cannot be crystallized. *E. coli* DHPR was reported as being a 120 kDa tetramer in solution (*5*), which we recently confirmed using native gel electrophoresis (*14*). While it is currently not possible to determine the NMR structure of such a large protein as DHPR, various NMR methods can be used to study protein−ligand interactions in solution for such large systems, especially using TROSY (transverse relaxation optimized spectroscopy) (*15*) and monitoring binding events using chemical shift perturbation studies (*16, 17*). Such studies can be complemented by saturation-transfer difference (STD) titrations to measure K_d values and to determine binding epitopes (*18*). This is the strategy taken in the study reported herein, to describe interactions between adjacent binding sites and between monomers in the DHPR tetramer.

MATERIALS AND METHODS

All NMR experiments were performed on a 600 MHz Varian NMR System instrument equipped with a triple resonance cryoprobe and *z*-axis gradients. An HP 8452A diode array UV−vis spectrophotometer was used for determining DHPR concentration and for coupled enzyme assays. All NuPage and Novex reagents and gels for the SDS-PAGE analysis are from Invitrogen. Salts, buffers and other chemical reagents (including NAD^+, NADH and PDC) are from Sigma-Aldrich and are of biochemical reagent grade. Protein concentrations were determined with the Bradford assay using the Bio-Rad protein assay kit from Pierce. All titration data were fitted using SigmaPlot (Version 8.0) software.

Expression and Purification of E. coli DHPR. *E. coli* DHPR and dihydrodipicolinate synthase (DHPS) were expressed from *E. coli* (BL21) and purified following previously described methods (*14*). DHPR purity and mass were verified by SDS-PAGE (28 kDa) and MALDI-TOF (28 821 Da, observed; 28 756 Da, expected), and enzyme activity was verified using a DHPS-coupled enzyme assay, as described previously (*14*).

Expression and Purification of ^{2}H, ^{15}N,^{13}C-labeled E. coli DHPR. BL21 cells containing the *E. coli* pET11a expression construct were grown in 1 L 2YT media to an OD_{600} of 0.7, spun down by centrifugation at 7000 rpm for 5 min then washed twice with deuterated M9 media (99.9% D_2O). Cells were then resuspended in 250 mL M9 media containing 48 mM Na_2HPO_4, 22 mM KH_2PO_4, 8.6 mM NaCl, 23 mM $^{15}NH_4Cl$ and 0.3% D-glucose-$^{13}C_6$-1,2,3,4,5,6,6-d_7. To this was added 124 mg of $MgSO_4 \cdot 7H_2O$, 3.7 mg of $CaCl_2 \cdot 2H_2O$ (filtered with a 0.2 μm filter), 250 μL of trace element stock (620 μM $FeCl_3$, 6.3 μM $ZnSO_4$, 6.4 μM $CuSO_4$, 6.7 μM $MnSO_4$ and 7.6 μM $CoCl_2$), 250 μL of 0.5 mg/mL carbenicillin stock and 2.5 mL of basal vitamin mix (GIBCO, MEM vitamin solution, 100×). After the cells were grown for 1 h at 37 °C, 500 μL of a 0.4 M IPTG stock was added (final 0.8 mM) to start induction. Cells were grown at room temperature overnight then collected, lysed and protein was purified using a 75 mL QA52 anion exchange column and a Blue Trisacryl affinity column with gravity gradient chromatography. Fractions were analysized using SDS-PAGE analysis, then pooled and concentrated using a 400 mL Amicon ultrafiltration device with YM10 membrane (Millipore). Desalted and concentrated fractions were loaded onto the Blue Trisacryl affinity column and eluted with a linear gradient of 0−2 M NaCl, 25 mM Tris buffer (pH 7.5). DHPR fractions were again pooled, concentrated and buffer exchanged. The DHPR solution was then flash frozen in liquid nitrogen and stored at −80 °C until use. Before using, DHPR was thawed on ice and enzymatic activity evaluated using a coupled assay, as described previously (*14*). Total yield of triple labeled DHPR was 130 mg. The SDS-PAGE analysis of triple labeled DHPR is provided in Supporting Information Figure S1. The triple labeled *E. coli* DHPR was used in $^{1}H-^{15}N$ HSQC titration experiments, and ^{13}C label permitted HNCO analysis as needed (Supporting Information, Figure S2).

Preparation of NMR Samples. For STD (saturation transfer difference) titration studies, all stocks including 50 mM NAD^+, 50 mM NADH, 50 mM PDC, 4 mM CRAA and 1 mM *E. coli* DHPR were prepared in 25 mM phosphate D_2O buffer, pH 7.8 (this measured pH was not corrected for the isotope effect at the electrode). Due to the inherent instability of the DHP substrate, binding interactions in the substrate site could only be probed using the PDC analog. The *E. coli* DHPR concentration in the STD study was 20 μM, and ligand concentrations were increased from 50 μM to 2000 μM (Figures 2, 3, 4, and 5). The NAD^+ and NADH were freshly prepared before experiments, and the concentrations monitored carefully using UV−vis spectroscopy. The NAD^+ concentration was monitored by reaction with 1 M sodium cyanide, and detecting the addition product with absorbance at 325 nm and $\varepsilon^{325} = 6.22$ mM/cm (*19*). The NADH concentration was monitored based on absorbance at 340 nm ($\varepsilon^{340} = 6.22$ mM/cm). Titration experiments were designed to be run in a single sample tube, ensuring that total added sample volume was never greater than 10% of the starting sample volume.

For the $^{1}H-^{15}N$ HSQC titration studies (Figures 6−11), all stocks were made in 25 mM d_{11}-Tris 10% D_2O buffer, pH 7.8, including 20 mM NAD^+, 20 mM NADH, 20 mM PDC, 4 mM CRAA and 0.8 mM triple labeled *E. coli* DHPR. Again, the NAD^+ and NADH were freshly prepared and their concentrations were monitored as above. In the $^{1}H-^{15}N$ HSQC experiments of the triple labeled DHPR, the deuterium

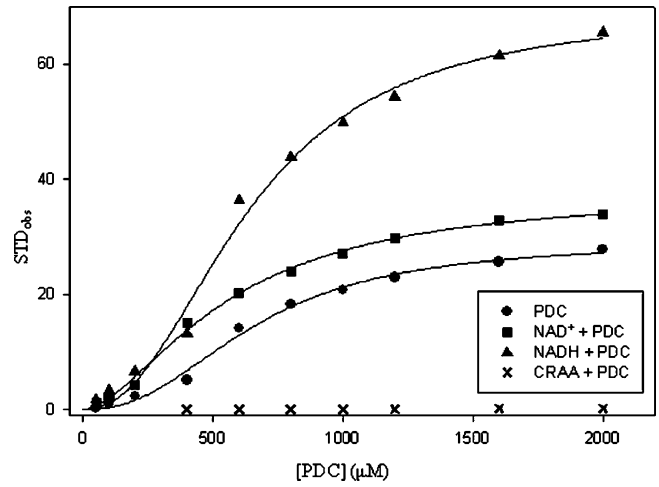

FIGURE 2: STD titration of DHPR complexes with PDC. Titration was of DHPR alone and DHPR saturated with NAD^+, NADH and CRAA, separately. The STD intensity for the PDC single peak (three aromatic protons are degenerate to a single peak) at 8.0 ppm were recorded and fitted to $STD_{obs} = -STD_{max}/(1 + ([PDC]/K_d)^n) + STD_{max}$, where n is the Hill coefficient.

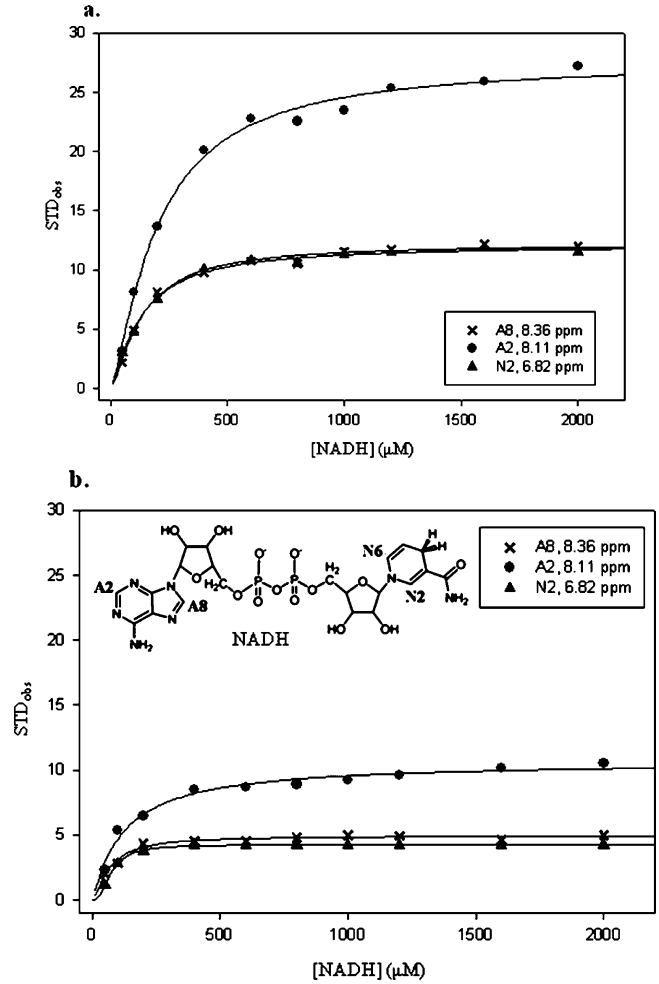

FIGURE 3: STD titration of DHPR (±PDC) with NADH. STD intensities were recorded for three NADH protons, and fitted to the equation: $STD_{obs} = -STD_{max}/(1 + ([NADH]/K_d)^n) + STD_{max}$. (a) STD titration of DHPR with NADH without PDC bound. (b) STD titration of the DHPR·PDC complex with NADH. The inset is the NADH structure with A8, A2 and N2 protons assigned.

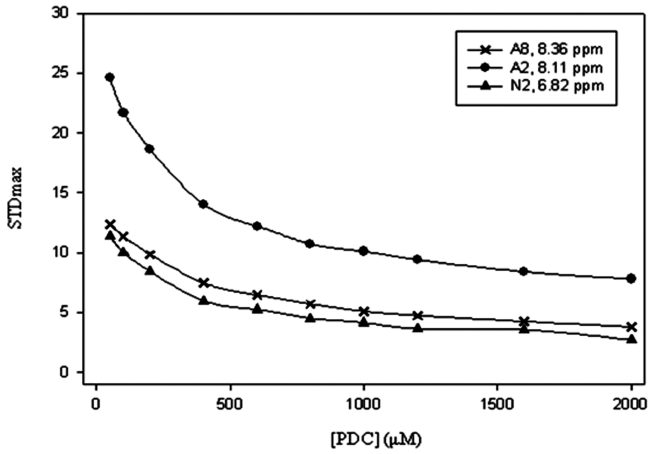

FIGURE 4: NADH STD signal intensity as a function of PDC concentration. Different STD_{max} values indicate different binding epitopes for NADH, depending on the presence of PDC. NADH was present at 2 mM and DHPR at 20 μM, so the DHPR·NADH binary complex was present throughout the titration.

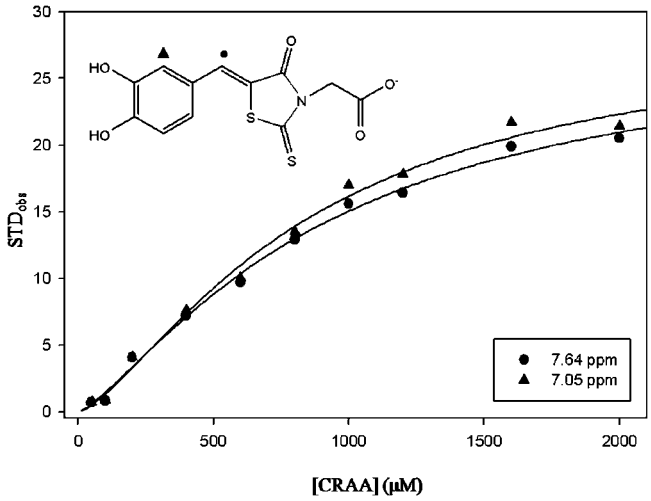

FIGURE 5: STD titration of DHPR with CRAA. Two proton intensities were plotted as a function of CRAA concentration. Data were fitted to $STD_{obs} = -STD_{max}/(1 + ([CRAA]/K_d)^n) + STD_{max}$.

on carbon was present to increase S/N by decreasing dipolar relaxation effects, along with use of TROSY. ^{13}C label was included to permit acquisition of 3D HNCO spectra to resolve spectral overlap in the $^1H-^{15}N$ HSQC spectra, but S/N was not adequate for such studies (see Supporting Information, Figure S2).

STD Titrations of E. coli DHPR with its Ligands. STD NMR studies were recorded at 298 K and were performed using the Varian cyclenoe pulse sequence. 1D ^1H NMR spectra were always collected before the NOE experiment in order to monitor and verify the ligand concentrations, to be sure that concentration increases linearly in the titration, as expected (i.e., there is no precipitation). During the STD experiment, alternating on-resonance irradiation of the protein methyl region (around 0.85 ppm), and off-resonance irradiation in a region distal from any protein or ligand signals (−10.8 ppm), was used. The *tof* value (carrier frequency) was set on water (4.76 ppm), and eight steady-state scans were used to bring the sample to thermal equilibrium in the presence of Rf-heating from the saturation process. The *spacing* and *pattern* values were set at 20 and 5, respectively. *Cycle* was set to y and *tau* to 100 ms, with *satpwr* (saturation

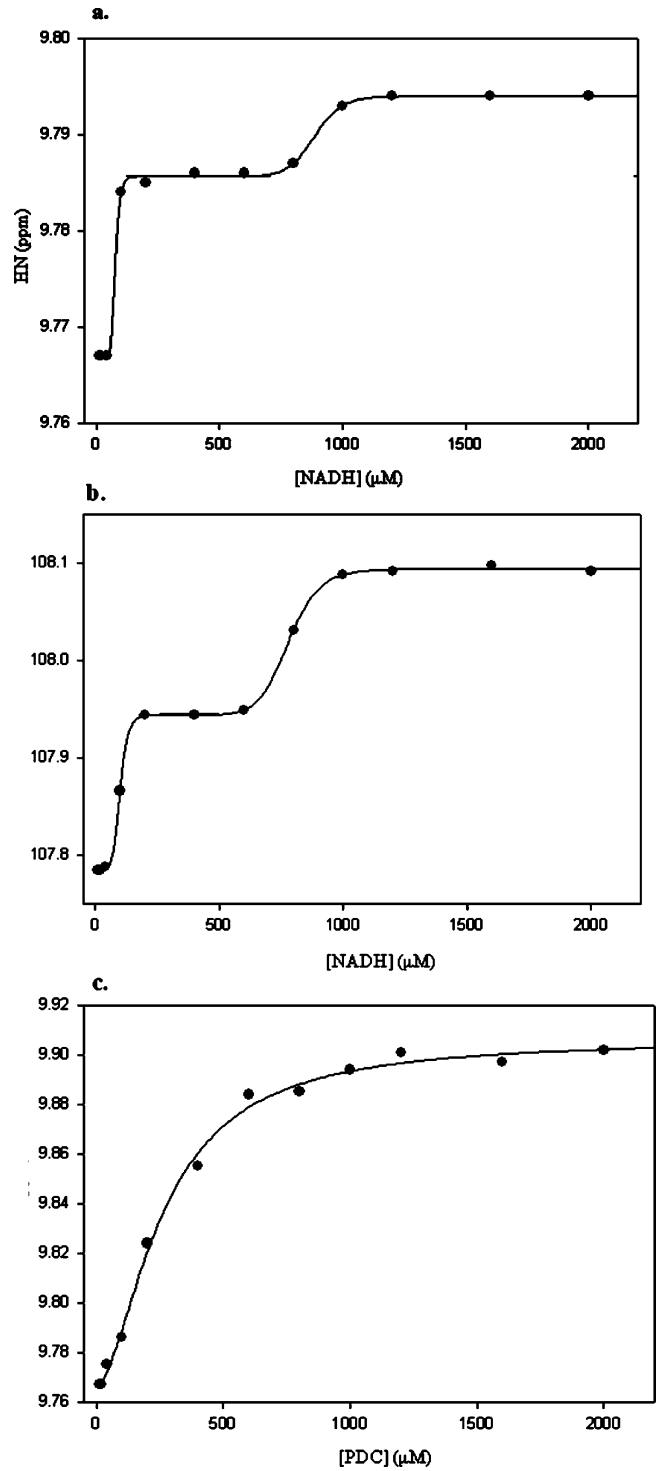

FIGURE 6: Plots of $^1H-^{15}N$ HSQC titration data for DHPR. Titration with NADH, (a) plotting amide HN (9.767, 130.783) versus NADH concentration, or (b) plotting ^{15}N chemical shift of cross peak (7.632, 107.792) versus NADH concentration. (c) Titration with PDC, plotting amide ^{15}N (9.766, 130.766) versus PDC concentration. The chemical shift change is fitted to equation: $\Delta\delta = \delta_{min} + (\delta_{max} - \delta_{min})/(1 + (K_d/[ligand])^{Hillslope})$ for ligand binding with sigmoidal dose−response (variable slope). In each spectrum, DHPR was present at 800 μM. Note that when fitting data for titrations when [ligand] ≤ [protein], curves indicate only binding stoichiometry.

power) at −10 dB. Total irradiation time (*sattime*) was 4 s, with 64 transients collected per experiment. All 1D ^1H NMR spectra and 1D STD difference spectra were processed using Varian VnmrJ software on a Linux workstation. Exponential

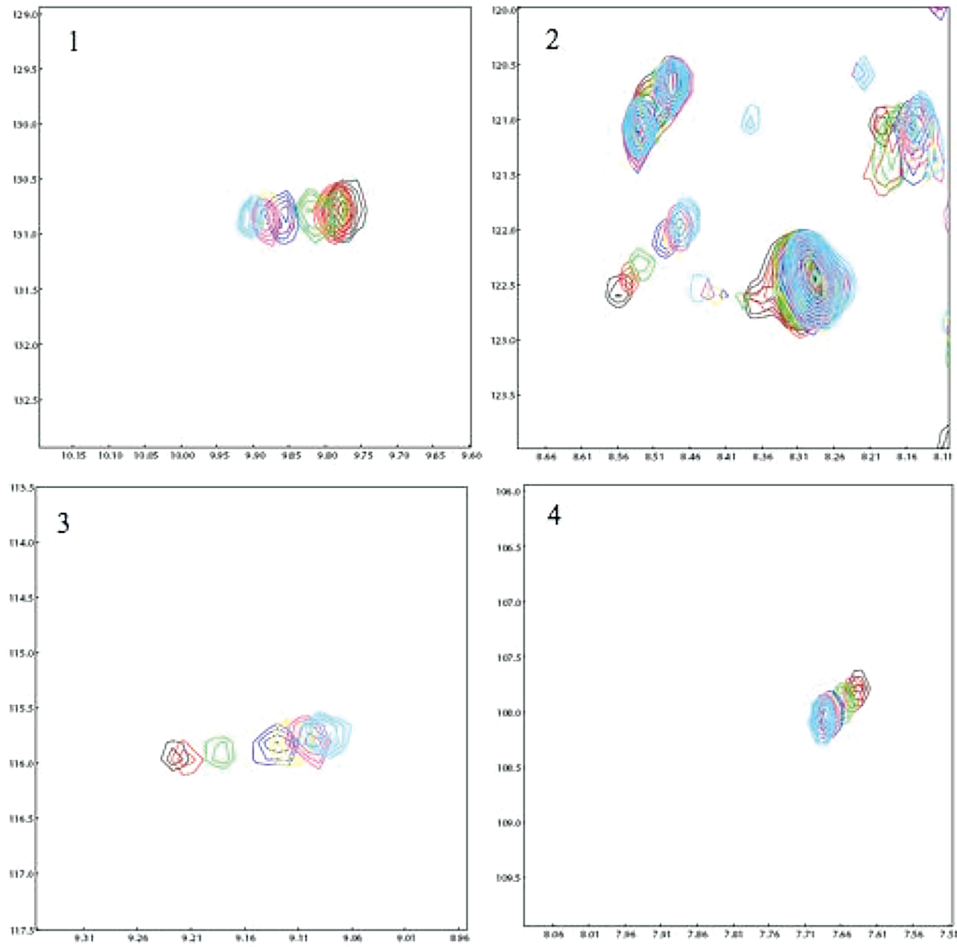

FIGURE 7: Overlay of 2D $^{1}H-^{15}N$ HSQC spectra (expansions for four crosspeaks) for the titration of DHPR with PDC. Full spectrum is in Supporting Information. DHPR was present at 800 μM and PDC was present at 40 (black), 100 (red), 200 (green), 400 (blue), 600 (yellow), 800 (magenta) and 2000 (cyan) μM. Peak #1 is from Trp253.

multiplication was used with 2 Hz line broadening, and care was taken to maintain a constant vertical scale (vs) for intensity determinations. All other STD titration data were normalized to this data set, if different conditions were used, such as number of transients collected.

$^{1}H-^{15}N$ HSQC Titrations of $^{2}H,^{15}N$-labeled E. coli DHPR. $^{1}H-^{15}N$ HSQC (TROSY) NMR titration experiments were performed with deuterated, ^{13}C and ^{15}N labeled DHPR samples (^{13}C-labeling is not used in this case) at 298 K on a 600 MHz Varian spectrometer equipped with cryoprobe. The *tof* value was again set at the water frequency (4.76 ppm). For each experiment, 1024 × 128 complex data points were acquired with 32 scans and a recycle delay of 1.0 s, resulting in experiment times of ~2 h. The two-dimensional TROSY-HSQC NMR spectra were processed using NMRPipe and analyzed with NMRView. ^{1}H chemical shifts in every spectrum were referenced to the water proton resonance at 4.76 ppm (at 298 K), while ^{15}N shifts were referenced indirectly, based on the ratios of gyromagnetic ratios. Processing in each dimension was with a 90° shifted sine bell window function.

RESULTS

STD Titration of DHPR with PDC. The *E. coli* DHPR ligand binding processes were first studied using STD-based titrations. Such titrations will reflect binding based on signal from magnetization transfer from protein to ligand, for ligands that bind in fast exchange. The substrate analog PDC binding occurs with positive cooperativity ($n \approx 2$), whether NADH or NAD^{+} is present or not (Figure 2 and Table 1). While STD-based titrations are increasingly being used to obtain K_d values for protein−ligand complexes, there are no published examples (to our knowledge) where these titrations were used to obtain Hill coefficients. Although, as in any titration where protein or ligand properties are monitored based on fractional saturation (ex. monitoring fluorescence signal), extraction of Hill coefficients should not depend on the biophysical method used to measure fractional saturation of the protein, other than to the extent that different methods may measure different aspects of the binding process (ex. from the protein or ligand perspective). Still, given this potential concern, we performed the titration of DHPR with PDC using a complementary and more widely used technique, by monitoring tryptophan fluorescence from DHPR (see Supporting Information). This fluorescence-based titration indicates that PDC does indeed bind with positive cooperativity, albeit with a slightly lower Hill coefficient ($n \approx 1.5$) than that obtained using STD-based measurements.

In our STD titrations, the binding affinity of PDC was not affected by the presence of NADH or NAD^{+} ($K_d = 0.6$ mM), but the presence of cofactor does change the STD_{max} of PDC. NADH showed the greater effect on the PDC binding profile, increasing the PDC STD_{max} from 29.1 to

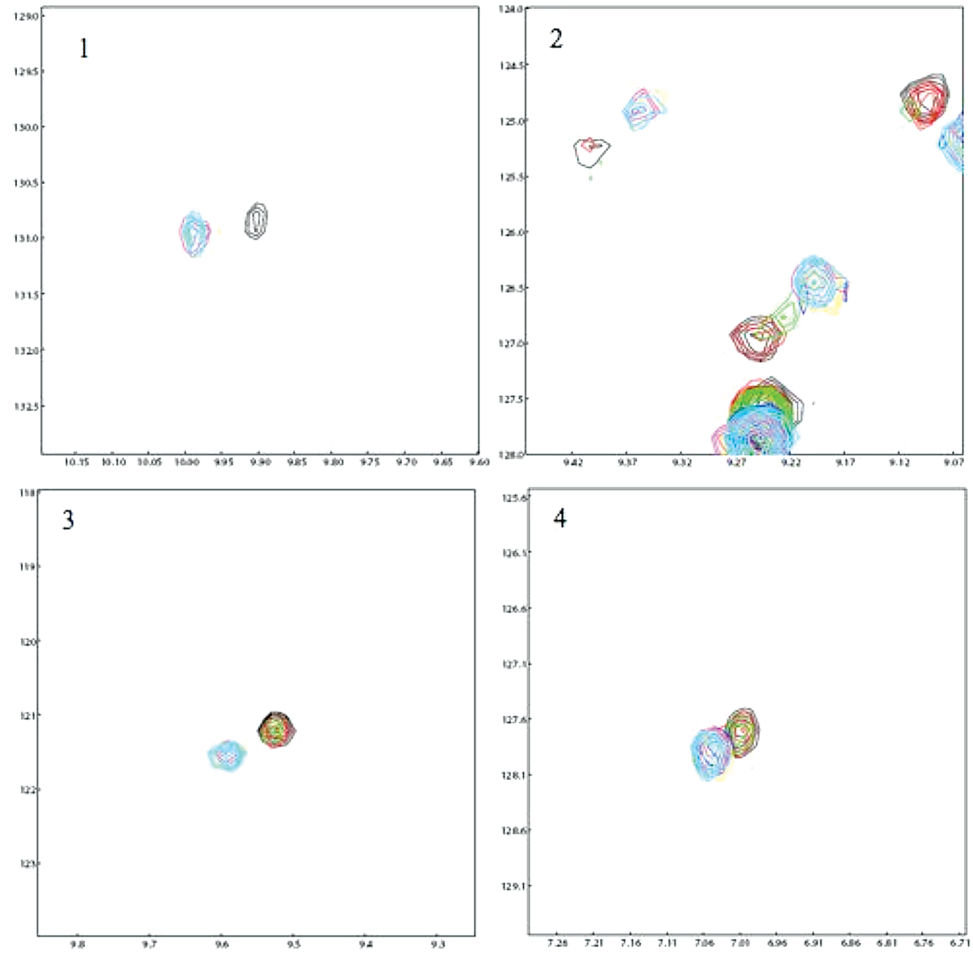

FIGURE 8: Overlay of 2D $^{1}H-^{15}N$ HSQC spectra (expansions for four crosspeaks) for the titration of the DHPR·PDC complex with NADH. Full spectrum is in Supporting Information. DHPR was present at 800 μM, PDC was present at 2000 μM and NADH was present at 0 (black), 20 (red), 40 (green), 100 (blue), 200 (yellow), 400 (magenta) and 800 (cyan) μM. Peak #1 is from Trp253.

69.4. NAD^+ showed a smaller effect on PDC binding, only increasing the PDC STD_{max} from 29.1 to 37.8. One interpretation of these changes is that NADH induces a larger conformational change, which results in the PDC molecule becoming more buried in the ternary complex; in contrast, NAD^+ binding permits a more open structure around the PDC site. An alternative explanation for these changes in STD_{max} is that NADH induces a conformational change that alters the rate of exchange (binding/release) for PDC, such that exchange occurs faster in the complex with NADH than in the complex with NAD^+, or with no cofactor present. Given HSQC results suggesting slower conformational exchange in the ternary complexes (vide infra), the former interpretation is favored (furthermore, PDC binds relatively weakly). Another observation from Figure 2 is that when DHPR was saturated with CRAA (an NADH competitive inhibitor), the PDC STD signal was negligible, indicating that PDC may prevent CRAA binding.

STD Titration of DHPR with NADH with or without PDC Present. When *E. coli* DHPR was titrated with NADH, the NADH protons showed different STD_{max} values for its resolvable adenine (A2, A8) and nicotinamide ring (N2) protons (Figure 3), indicating NADH binds with a topography with some protons more buried than others. The Hill coefficient indicates that NADH binding, unlike PDC, is not cooperative (Table 2). However, it should be noted that if some monomer site(s) bind NADH with very high affinity, binding would not be in fast exchange and would therefore be invisible to STD titrations. In this regard, ITC studies have been reported where NADH K_d was <1 μM. The K_d values reported herein for NADH are 70−200 μM (Table 2). Binding affinity for NADH was about 2-fold greater for the DHPR·PDC binary complex than for binding to DHPR (Figure 3 and Table 2). This indicates weakly synergistic binding between PDC and NADH. Furthermore, in the titration of the DHPR·NADH complex with PDC, STD_{max} for NADH decreased as PDC concentration increased (Figure 4). This is again consistent with a change in conformation induced by PDC binding (see Figure 12) whereby the NADH becomes somewhat less buried in the protein. But, as noted earlier in the case of PDC, an alternative explanation must also be considered, whereby PDC binding alters the exchange dynamics for NADH binding, such that exchange is slower in the presence of PDC. This would be consistent with HSQC dynamics data (vide infra), so is the favored interpretation in this case.

$^{1}H-^{15}N$ HSQC Titration of DHPR with PDC. While chemical shift assignments are not available for DHPR, due to its size and poor quality 3D spectra (see 2D HNCO spectrum in Supporting Information, Figure S2), 2D $^{1}H-^{15}N$ HSQC spectra were of good quality. Such spectra permit studies of ligand binding events, enabling relative assessment of conformational changes based on crosspeak changes, as well as time scale (ex. fast vs slow exchange). While many

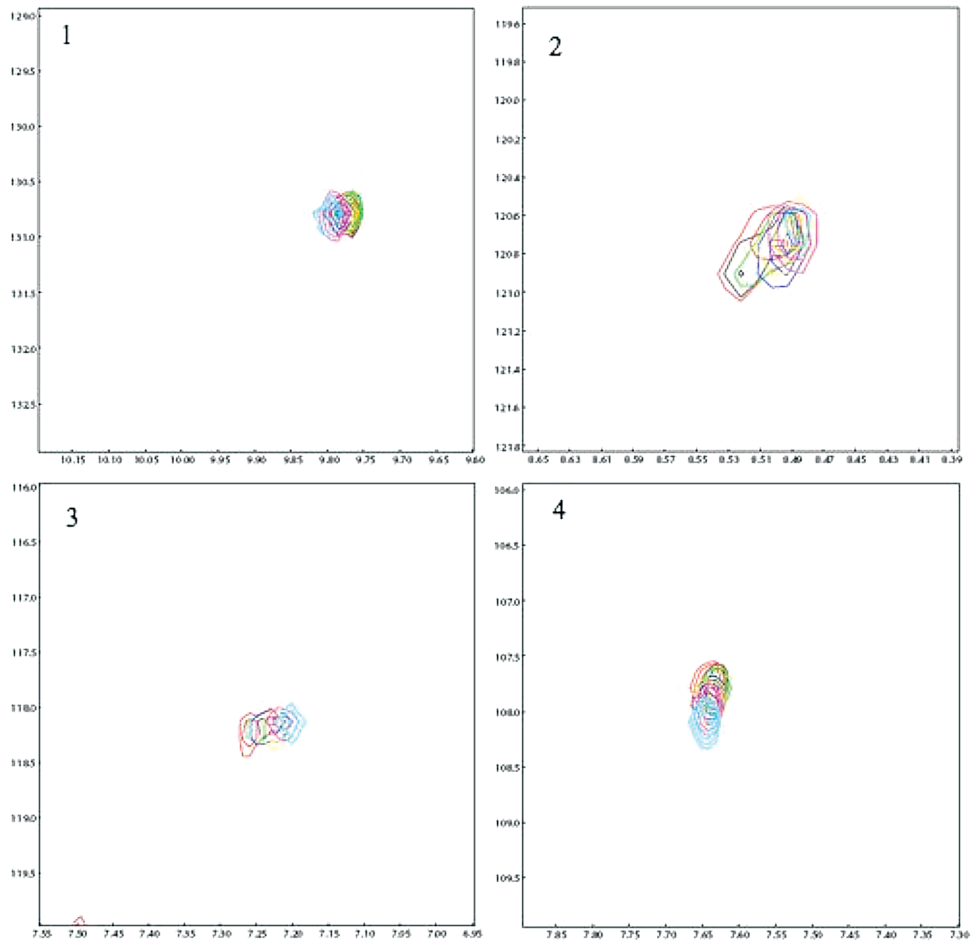

FIGURE 9: Overlay of 2D $^{1}H-^{15}N$ HSQC spectra (expansions for four crosspeaks) for the titration of DHPR with NADH. Full spectrum is in Supporting Information. DHPR was present at 800 μM and NADH was present at 0 (black), 20 (red), 40 (green), 100 (blue), 200 (yellow), 400 (magenta) and 2000 (cyan) μM. Peak #1 is from Trp253.

well-dispersed and sharp crosspeaks are observed, there are also a large number of missing crosspeaks, most likely due to exchange broadening effects; such effects would be expected if regions of structure were flexible and sampling multiple conformations on the msec timsecale, as might be expected for binding site residues and loop regions in DHPR. Many of the observed crosspeak changes are likely coming from the N-terminal domain which binds NADH. The C-terminal domain is involved in tetramer formation, forming a hydrophobic core of parallel β-sheets, which acts as a core structure around which the 4 Rossmann fold domains are positioned (Figure 13a,c,d). This core is less likely to be perturbed, unless conformational changes associated with binding cooperativity between monomers can occur. We observed that the titration of PDC caused significant chemical shift changes in DHPR (Figures 7 and 10), for certain crosspeaks. One residue of particular interest is Trp253, because it is at the interface of interacting monomers in the DHPR tetramer (see Figures 12 and 13). Furthermore, because there is only one tryptophan in DHPR, and Trp's have a unique downfield chemical shift, this residue can be assigned in Figures 7−11, and used as a measure of domain movement around the core (Figure 13). Besides chemical shift, this crosspeak can be assigned to the Trp side chain based on its not being observed in the 2D $^{1}H-^{15}N$ plane from the HNCO experiment, which would only show amide NHs (Supporting Information, Figure S2). Crosspeak changes could also be fitted to obtain K_d values if [ligand] > [protein], or at least binding stoichiometry if [ligand] < [protein] (Figure 6 and Supporting Information: Figure S3 and Table S1). In this regard, it is noteworthy that the Trp253 crosspeak shifts downfield in the ^{1}H dimension to a new state that is in fast exchange with that for apo DHPR. Fast exchange also appears to be occurring when NADH binds to apo DHPR as well, although chemical shift changes are smaller (Figure 9). This would indicate, based on the chemical shift changes, that the interconversion of states in Figure 1d (and represented in Figure 13) occurs with a rate constant $k_{ex} = 1/(1/k_R + 1/k_T) > 2.22*\Delta\delta$. Given the change in $\Delta\delta$ for Trp253 of 82.2 Hz for apo DHPR → DHPR·PDC (Figure 7), this makes $k_{ex} > 182\ s^{-1}$. Binding of the second ligand, whether NADH to DHPR·PDC (Figure 8) or PDC to DHPR·NADH (Figure 10), involves a slower exchange between states, with $k_{ex} < 120\ s^{-1}$ (DHPR·PDC ↔ DHPR·PDC·NADH) or $k_{ex} < 269\ s^{-1}$ (DHPR·NADH ↔ DHPR·NADH·PDC). This slow exchange in forming the ternary complexes was noted in our earlier interpretation of STD results.

$^{1}H-^{15}N$ HSQC Study of E. coli DHPR Binding with CRAA and PDC. We had previously reported that CRAA binds to the NADH cofactor site, based on steady state competitive inhibition studies versus NADPH (*13*) and later shown the same with a native in gel competition assay versus NADH (*14*). But, in $^{1}H-^{15}N$ HSQC titrations, PDC does not cause significant chemical shift changes of labeled DHPR for the DHPR·CRAA complex (Figure 11), consistent with CRAA preventing PDC binding, as observed also with the STD

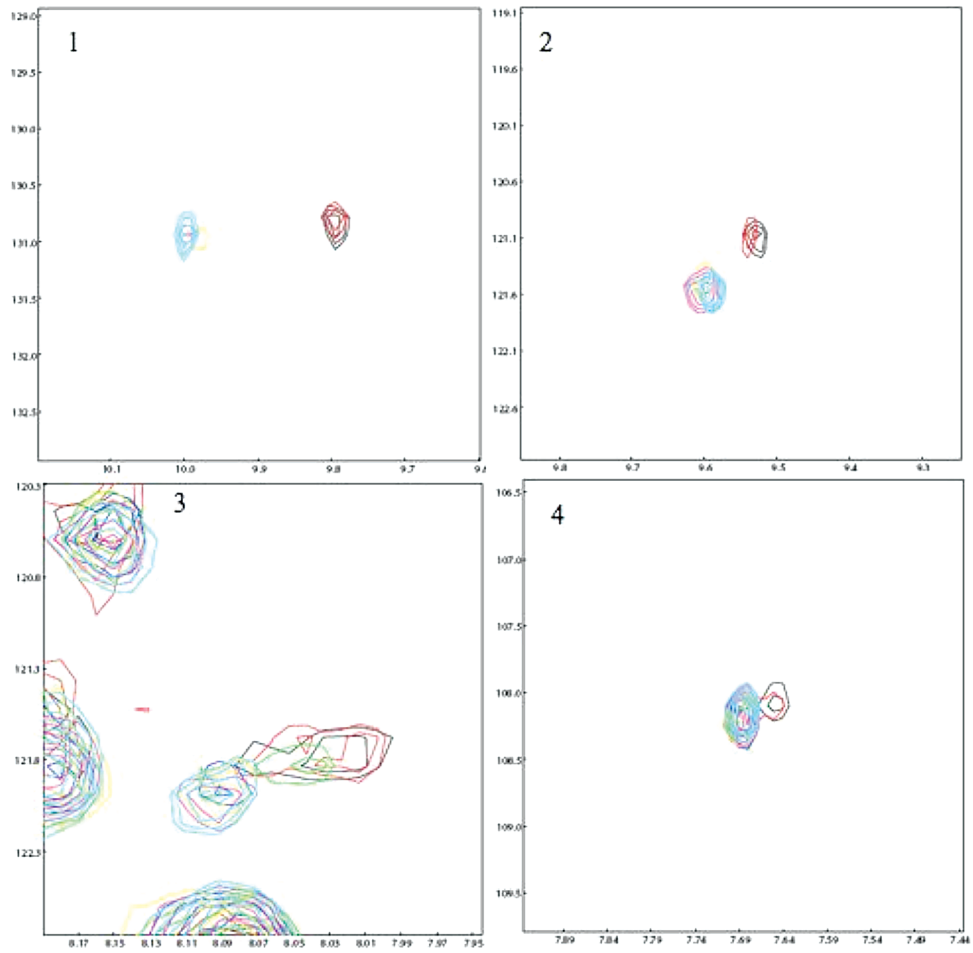

FIGURE 10: Overlay of 2D $^{1}H-^{15}N$ HSQC spectra (expansions for four crosspeaks) for the titration of the DHPR·NADH complex with PDC. Full spectrum is in Supporting Information. DHPR was present at 800 μM, NADH was present at 2000 μM and PDC was present at 20 (black), 40 (red), 100 (green), 200 (blue), 400 (yellow), 600 (magenta) and 2000 (cyan) μM. Peak #1 is from Trp253.

titration (Figure 2). Such results could have misled fragment assembly efforts by suggesting that CRAA binds in the PDC site, which is not the case. Finally, CRAA, like NADH, does not cause significant chemical shift perturbation in the HSQC spectral titration (Figure 11).

DISCUSSION

STD Titrations. Studies of DHPR binding to the substrate analog PDC and either NAD^+ or NADH were performed, to define synergy and cooperativity effects. DHPR binding of NADH and PDC should mimic formation of the catalytically competent Michaelis complex with NADH and substrate DHP. Conversely, the binding of NAD^+ and PDC is intended to mimic formation of the product complex with NAD^+ and THP (Figure 1a). STD-based titrations indicate that PDC binds with positive cooperativity ($n \approx 2$) to apo DHPR as well as to the complex with either NADH or NAD^+ present (Figure 2 and Table 1). This is consistent with the structure, which is a homotetramer with approximate 2-fold symmetry, and the appearance of a dimer of dimers (Figure 13 a). Accordingly, besides causing domain closure (Figure 12b), PDC binding may cause shifting of a monomeric unit around the tetrameric core—see for example the two monomers on the left side of Figure 13a, which both have PDC bound. This cooperative effect seems to be independent of cofactor, since the Hill coefficient is 2 in all cases.

In contrast to the situation with PDC, NADH binding shows little cooperativity in any of the complexes (Figure 3), and binding is with a relatively high K_d of 70−200 μM (Table 2). This was somewhat unexpected, because crystal structure analysis suggested some interactions between NADH pockets might occur, because DHPR crystallized with only three sites occupied (Figure 13a), consistent with negative cooperativity. Also, ITC titrations indicated a tight binding NADH with $K_d < 1$ μM. But, STD-based titrations only reflect fast-exchange binding processes, and only provide aggregate measures of binding events at multiple interacting monomeric sites (reflected in Hill coefficients). In contrast, HSQC titrations (vide infra) can potentially overcome both of these limitations, at least under some conditions, by showing all binding events.

In terms of interactions between substrate sites within a monomer, there is only weak binding synergy between PDC and NADH or NAD^+ cofactors. The NADH K_d decreases ~2-fold in the presence of PDC, and the PDC K_d is not significantly affected by the presence of NADH or NAD^+. This lack of binding synergy is in contrast to what is observed in the steady state, where an ordered sequential mechanism (*20*) has been reported (i.e., DHP substrate binds preferentially to the DHPR·NADH complex), and is shown in Figure 1b. This may be due to differences in binding interactions between substrate (DHP) and substrate analog (PDC), or to

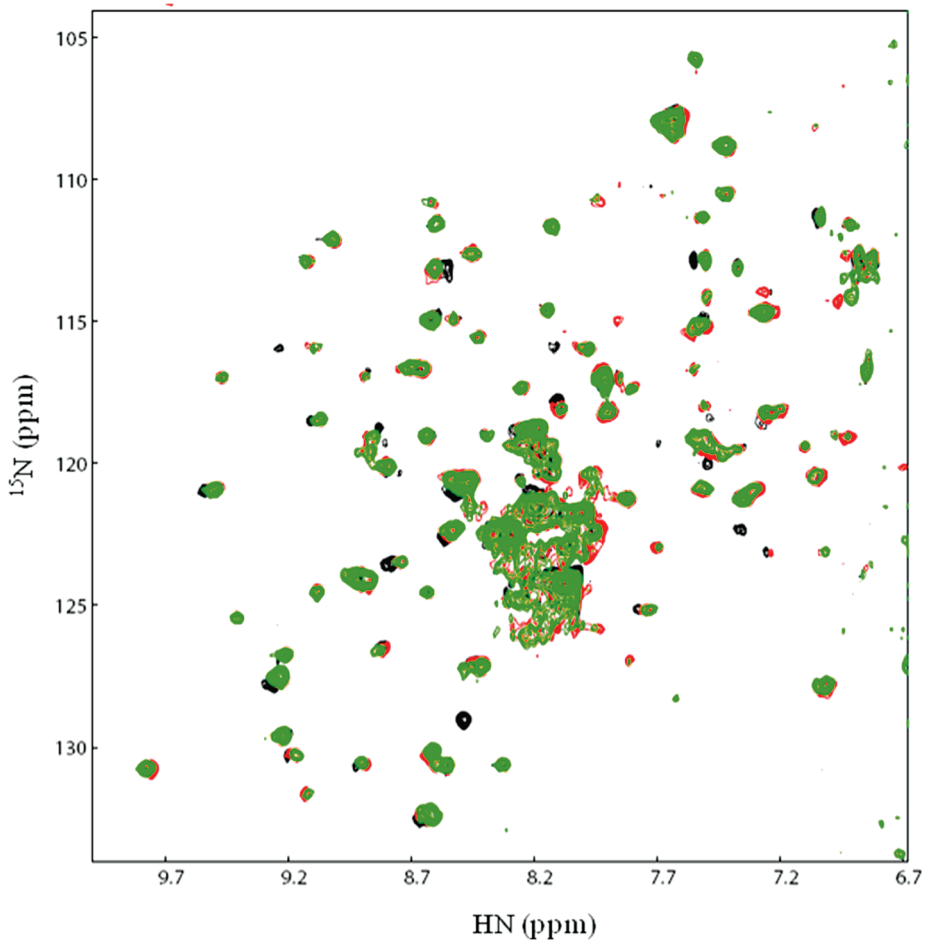

FIGURE 11: Overlay of 2D ^{1}H−^{15}N HSQC spectra of 0.8 mM DHPR (black), 0.8 mM DHPR + 2.0 mM CRAA (red) and 0.8 mM DHPR + 2.0 mM CRAA + 2.0 mM PDC (green).

Table 1: STD Analysis of PDC Binding to Various DHPR Complexes[a]

E. coli DHPR complex	STD_{max}	K_d (μM)	*n*	*R*
DHPR	29.1 ± 1.5	661 ± 40	2.4 ± 0.3	0.997
DHPR·NADH	69.4 ± 4.4	639 ± 52	2.2 ± 0.3	0.995
DHPR·NAD$^+$	37.8 ± 1.7	558 ± 40	1.7 ± 0.1	0.998
DHPR·CRAA[b]				

[a] *n* is the Hill coefficient and *R* is the correlation coefficient. The three PDC protons have degenerate chemical shift, so all three were monitored together in the titration. [b] At 2 mM PDC, STD_{obs} was still <0.14, indicating no significant binding.

Table 2: STD Analysis of NADH Binding to DHPR (± PDC)

(a) NADH Binding to apo DHPR[a]

peaks (ppm)	STD_{max}	K_d (μM)[b]	*n*	*R*
8.36	12.2 ± 0.3	134 ± 10	1.4 ± 0.1	0.995
8.11	27.6 ± 0.9	200 ± 17	1.3 ± 0.1	0.996
6.82	12.1 ± 0.3	130 ± 9	1.3 ± 0.1	0.992

(b) NADH Binding to the DHPR·PDC Complex[a]

peaks (ppm)	STD_{max}	K_d (μM)[b]	*n*	*R*
8.36	4.9 ± 0.1	68 ± 7	1.4 ± 0.3	0.979
8.11	10.6 ± 0.6	126 ± 20	1.1 ± 0.2	0.987
6.82	4.2 ± 0.02	76 ± 1	2.3 ± 0.1	0.999

[a] *n* is the Hill coefficient and *R* is the correlation coefficient. Protons are assigned in Figure 3. [b] K_d values should be the same for all three protons, so this variability reflects uncertainty in the measurements, most likely for the resonance at 8.11 ppm which had the largest error from fitting, and also deviated the most from the other two K_d measurements.

differences between steady state and NMR conditions (ex. protein concentration). Indeed, if there is a tighter binding NADH site that eluded detection by STD titrations, it might be the operative and more relevant interaction in the steady state.

While the above analysis indicates there is no binding synergy in terms of affinity, it does not address whether there are conformational changes induced preferentially by one or the other substrate, to facilitate formation of the Michaelis complex. Based on changes in STD_{max} for PDC (Figure 2), NADH binding appears to induce a conformational change that results either in (a) PDC becoming more buried in the protein, or (b) PDC exchange (binding/release) occurring faster in the ternary complex. As mentioned earlier, the former interpretation is favored in this case. Furthermore, since the STD_{max} for PDC binding to DHPR was increased more by NADH binding than NAD$^+$ binding (Figure 2), we propose that NADH triggers a closing down of the protein onto the substrate (Figure 12a); and, perhaps after NADH transfers the hydride to DHP and is converted to NAD$^+$, the enzyme opens up the substrate pocket somewhat, which would facilitate product release. Interestingly, there is an apparently opposite effect on NADH due to PDC binding, (Table 2 and Figures 3 and 4), where STD_{max} for NADH is lower in the ternary complex. Again, the two interpretations are that: (a) NADH is more solvent exposed in the ternary complex, or (b) NADH binding/release is slower in the ternary complex. In this case we favor the latter dynamics-based explanation for three reasons: (a) HSQC data indicate

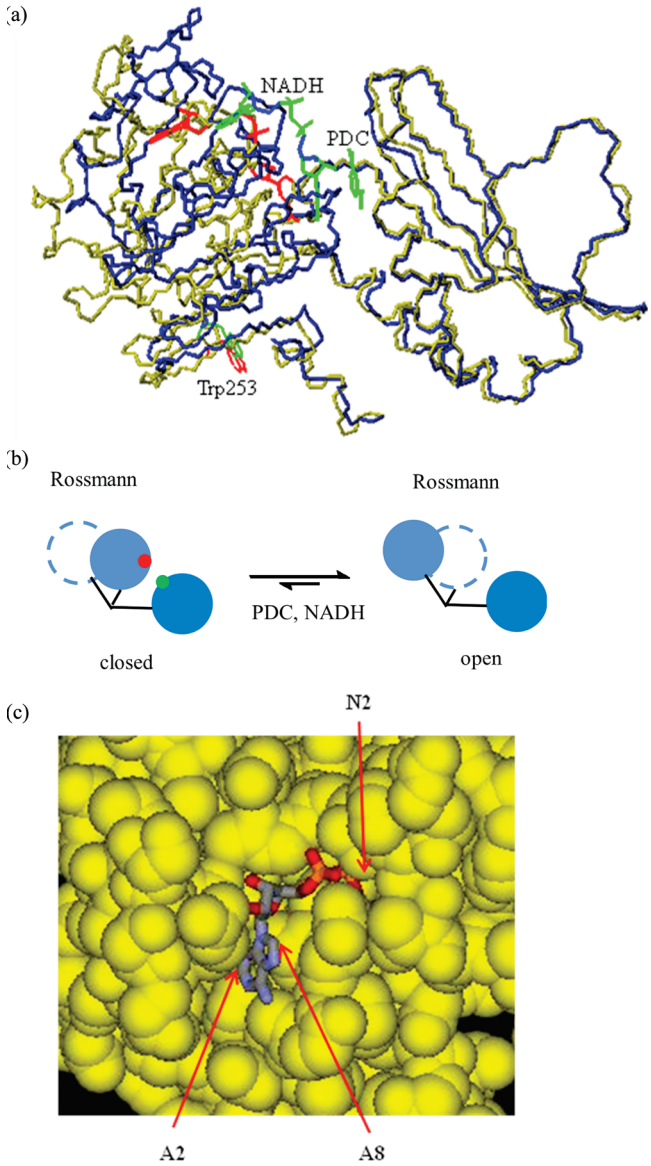

FIGURE 12: (a) Overlay of X-ray crystal structures of the DHPR binary complex with NADH (1DRU; yellow backbone) and the ternary E·NADH·PDC complex (1ARZ; blue backbone). NADH (green) and PDC (green) are visible at the interface of the Rossmann (left) and C-terminal (right) domains for the ternary complex; NADH (Red) in the binary complex is still bound to the Rossmann domain, but has now shifted away from the C-terminal domain. The NMR reporter residue, Trp253, is shown at the bottom left in red (1DRU) or green (1ARZ). (b) Cartoon representation of the conformational change induced by PDC binding, to bring the N- and C-terminal domains into proximity. (c) Expansion of the region around the NADH adenine and nicotinamide rings in the E·NADH·PDC ternary complex (1ARZ), showing the A2 and A8 adenine ring and N2 nicotinamide ring protons that were monitored in the STD titration (Figure 3).

protein conformational changes do indeed slow down in the ternary DHPR complex, relative to the binary complex (vide infra), (b) it seems unlikely that all three NADH protons would change how buried they were, to exactly the same extent, in going from binary to ternary complexes (see Figures 3 and 4), and (c) it would be unusual for the protein to "open up" upon formation of the Michaelis complex (although, this is possible).

Inspection of the crystal structure reveals that while PDC, which binds at the interface of the N- and C-terminal domains, becomes significantly buried in the ternary complex (Figure 13), the NADH is somewhat exposed in both open and closed states (Figures 12 and 13). While inspection of the crystal structure reveals which parts of the NADH molecule are more solvent exposed in one static conformation, STD_{max} values provide quantitative data for the solution state, which would also reflect the dynamic state of the protein (i.e., transient opening/closing of domains), to describe the regions that are exposed or are in more direct contact with protein (and might therefore have larger STD_{max}). STD_{max} values for the adenine (A2, A8) and nicotinamide ring (N2) protons on NADH (Figure 3) indicate that the A2 proton of the adenine ring is in more intimate contact with the protein relative to the A8 proton, consistent with the crystal structure shown in Figure 12c. As noted earlier, the preferred interpretation of the STD data for NADH (Figures 3 and 4) is that PDC binding causes a change in dynamics, such that binding/release of the NADH cofactor occurs more slowly in the ternary complex. This would also be consistent with HSQC data, which indicate slower time scale protein conformational changes are occurring in the ternary complex, compared to the binary complex.

Lessons from STD Studies for Fragment Assembly. Fragment-based drug discovery efforts led to the discovery of CRAA, which binds in the NADH pocket, and, when CRAA was tethered to PDC, a high affinity biligand inhibitor was obtained (*13*). In order to engineer a more potent biligand inhibitor, and to be able to identify new fragments to replace PDC (which does not penetrate bacterial cell walls), it is important to know if there is binding cooperativity and/or synergistic binding between the CRAA and PDC ligands. Besides affecting affinity of the biligand, synergistic binding might affect screening efforts to identify other DHP mimics (besides PDC). STD titrations of DHPR with CRAA indicate that it, like the NADH substrate it mimics, binds with little or no cooperativity (Figure 5, Table 3). Again, STD titrations only reflect binding processes that are in fast exchange, and this could explain the discrepancy with our previous report of cooperative binding for CRAA inhibition in the steady state (*13*). But, the STD titration with CRAA, when PDC is present (Figure 2), indicates that the DHPR complex with CRAA does not appear to bind PDC. This is surprising, since CRAA is known to bind in the NADH pocket, not the PDC pocket (*13*). But, because the CRAA carboxylic acid and the PDC dicarboxylate are negatively charged, the charge repulsion between these two ligands could cause a significant reduction in affinity for PDC, such that PDC would not bind in the presence of CRAA, even though they occupy different binding sites. This indicates that if CRAA is to be bound to DHPR when screening for adjacent binding fragments (PDC replacements), the negative charge will have to be neutralized to avoid negatively synergistic interactions that might prevent discovery of new PDC analogs. Indeed, the initial discovery that PDC and CRAA could be tethered to make a biligand inhibitor (*13*) was made using a neutral (propylamide) analog of CRAA in the ternary complex.

$^{1}H-^{15}N$ HSQC Titrations. From $^{1}H-^{15}N$ HSQC (TROSY) titrations, we observe that NAD(H) cofactor binding and PDC ligand binding cause related conformational changes in DHPR (see especially Trp253, which is affect by both ligands), although PDC appears to induce more dramatic

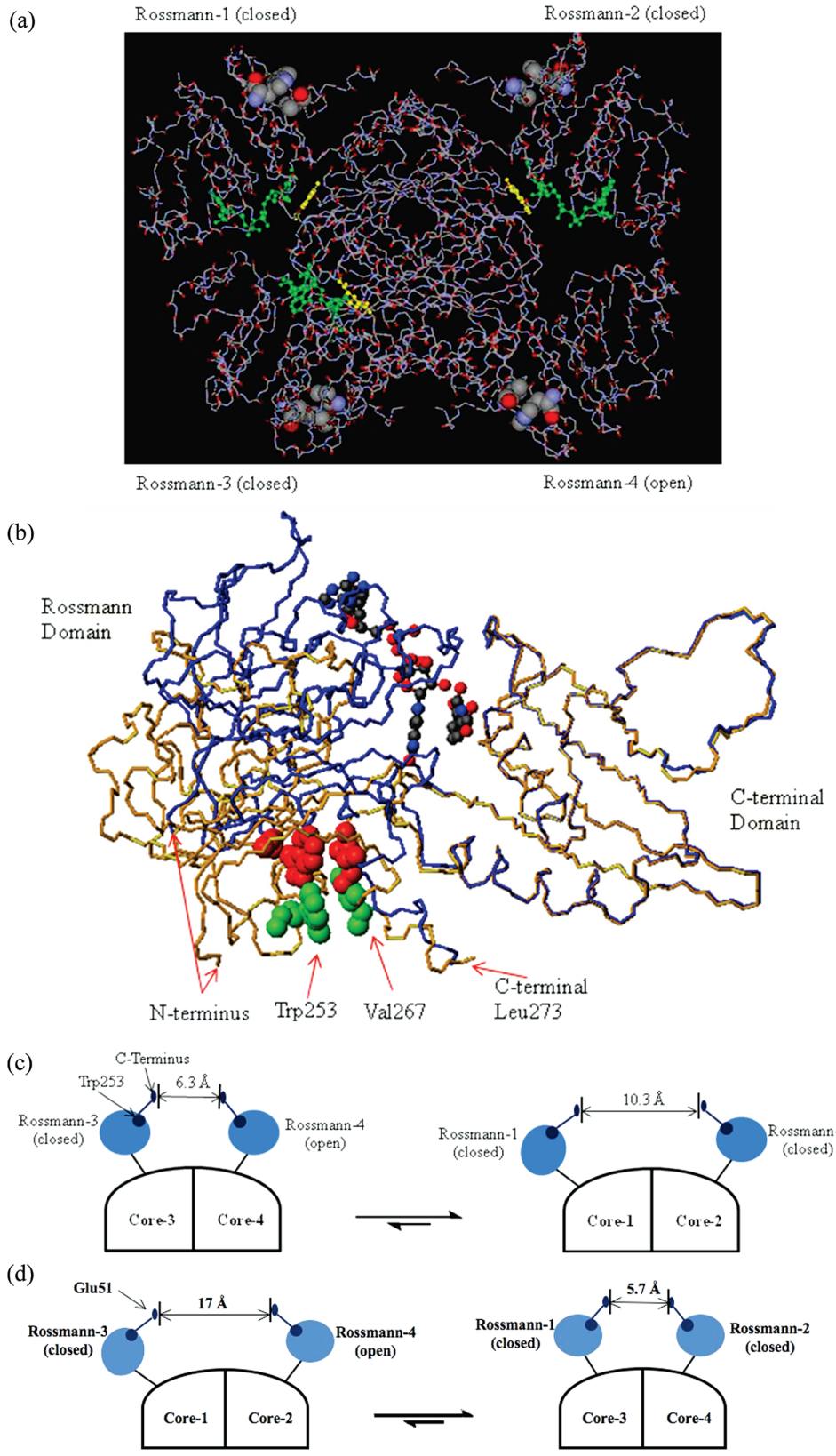

FIGURE 13: X-ray crystal structure showing the DHPR tetramer for the ternary complex with PDC/NADH (1ARZ) (a). The Trp253/Val267 stabilizing interaction is shown as a spacefill rendering in the tetramer (a) or isolated monomer (b). Between monomers in the tetramer, the C-terminal carbonyls in the closed/closed monomer pair (bottom) are 10.3 Å apart, and are 6.3 Å apart in the closed/open monomer pair (top). Likewise, the Trp253 indole nitrogens are 40.7 Å apart in the closed/closed monomer pair (top), and are 37.6 Å apart in the closed/open monomer pair (bottom). (b) Overlay of the "open" monomer (gold) and 'closed' monomer (blue) bound to NADH and PDC (rendered as ball-and-stick). The corresponding Trp253 and Val267 are shown in green (open) and red (closed). (c) Cartoon model showing how the N-terminal Rossmann domains shifted around the central N-terminal core domains, depending upon whether monomers are in "open" or "closed" conformations; effects on a small C-terminal loop region are shown. Distances are from the crystal structure of the ternary complex, so had three monomers in a "closed" conformation and one in an "open" conformation. Model shows only two of the four monomers at once. (d) Cartoon model as in panel (c), but showing intermonomer distance changes for Glu51.

Table 3: STD Analysis of CRAA Binding to DHPR[a]

peaks (ppm)	STD_{max}	K_d (μM)	n	R
7.64	28.3 ± 2.9	910 ± 160	1.3 ± 0.1	0.998
7.05	28.7 ± 3.4	840 ± 160	1.4 ± 0.2	0.996

[a] n is the Hill coefficient and R is the correlation coefficient. Protons are assigned in Figure 5.

chemical shift changes (Figures 7, 8, 9, and 10). Since it is clear from the structure (Figure 13) that domain movement associated with binding synergy would also lead to altered interactions between monomers, it is not surprising then that we had also observed more significant cooperativity for PDC binding (Figure 2), relative to NADH binding. Movement of the N-terminal Rossmann fold domain (triggered by PDC binding) would alter interactions between monomers, according to Figure 13. This cooperativity interaction is seen both at the top/bottom (Trp253) monomer interface in Figure 13a (schematically represented in Figure 13c), as well as the left/right interface in that same figure (schematically represented in Figure 13d).

We had noted above that fitting of STD data to obtain K_d values indicated only weak synergy between PDC and NADH binding. Interestingly, analysis of HSQC spectra indicates that when either of the two active sites is occupied, that first ligand binding event causes the protein to switch from fast exchange between two conformational states (with $k_{ex} > 182\ s^{-1}$) to intermediate or slow exchange, with $k_{ex} < 120\ s^{-1}$ (DHPR·PDC ↔ DHPR·PDC·NADH) or $k_{ex} < 269\ s^{-1}$ (DHPR·NADH ↔ DHPR·NADH·PDC). This suggests an increased kinetic barrier between open and closed states for the second binding event relative to the first, and provides an explanation as to why the STD_{max} values for the three NADH protons uniformly decreased (Figure 4) when PDC was added to form the ternary complex (i.e., there was a change in binding dynamics for NADH, rather than a change in how buried the cofactor was). This effect is best observed by monitoring the Trp253 residue that is present between monomers (Figure 13), and which serves as a reporter crosspeak (Figure 7) that was used to obtain k_{ex} estimates. This residue is not near either substrate binding site (Figure 12a), so will reflect only global conformational rearrangement, and movement of monomers around the core C-terminal domain in response to ligand binding events (Figure 13c). That this residue is perturbed and samples multiple states is consistent with monomer reorientation between two states (R⇌ T) during binding, as indicated in the crystal structure showing 3 monomers in a closed state (ternary complex) and one in the apo, open state (Figure 13a), with changes to Trp253 indicated (Figure 13b,c). Inspection of this crystal structure reveals that the N-terminal Rossmann domain shifts by 4 Å around the core domains, due to active site occupancy that may be related to cooperativity. Trp253 should be an effective reporter for this change, because the C-terminal domain emerges from the core at Ser239/Arg240 and packs up against the ligand-binding Rossmann domain with a 35 residue stretch that folds back onto itself, via stabilizing interactions between Trp253 and Val267 that orients the C-terminus toward the adjacent monomer (Figure 13). The HSQC titration data can be interpreted in light of these structures (Figures 12 and 13), and this reporter residue for monomer movement (Figure 13b,c). While NADH binding to the DHPR·PDC binary complex results in modest chemical shift perturbations (Figure 8), it induces somewhat larger chemical shift changes when binding to apo DHPR (Figure 9). This suggests that NADH can only induce monomer rearrangement when PDC is present, and even then it is a relatively small change - consistent with relatively little NADH cooperativity (Figure 3, Table 2). In contrast, PDC induces large chemical shift changes both for binding to the apo DHPR (Figure 7) and to the DHPR·NADH binary complex (Figure 10). These data indicate that PDC is primarily responsible for inducing monomer rearrangement (Figure 13c) associated with cooperativity, especially in forming the ternary complex. This would be consistent with observed cooperativity (Hill coefficient ≈ 2; Figure 2, Table 1) for PDC binding.

While the HSQC titrations of DHPR with NADH or PDC reveals little about affinity because, unlike in the STD titrations, ligands were not present in excess over protein (see Supporting Information), they do define binding stoichiometry. The titration in Figure 6 clearly shows there are two cofactor binding events, with the first occurring at 1 equiv of added NADH and the second binding occurring at ~3 NADH equiv. This first higher affinity binding event was not observed in the STD titration, most likely because it is in slow exchange. Indeed, ITC data had indicated a K_d of 0.46 μM for NADH (*6*), and steady-state kinetics had indicated a K_m of 1.6 μM for NADH (*20*). Interpretation of our HSQC titration data, in light of the previously reported steady state results, suggest that this first NADH binding event is the catalytically relevant one, and that the later and lower affinity binding events do not lead to formation of the Michaelis complex.

These data are consistent with the cooperativity model in Figure 1d, and with the intermediate state of the tetramer being the one on the path to the Michaelis complex. Notably, this model would now make our data consistent with the previously reported ordered sequential mechanism (Figure 1b), with NADH binding first and with higher affinity. That the apo DHPR tetramer binds one NADH with much higher affinity than the other three sites is also intriguing in light of previous crystal structure data that show, in the ternary complex, three monomers have both sites occupied, with the fourth being vacant (Figure 13a). What can explain this apparent reversal of stoichiometry, in comparing the crystal structure of the ternary complex (1(open):3(closed)) to results of the NMR titration data indicating first formation of the (higher affinity) NADH binary complex (3(open):1(closed))? And if the first NADH binding event is the catalytic *priming step*, then what is the relevance of the subsequent NADH binding events? Further studies will be needed to address this reversal of stoichiometry. In addition to considering NADH binding stoichiometry, we also note that initial PDC binding occupies no more than two of the four monomers in the first binding step, based on the curve inflection at 400 μM (Figure 6c), since 800 μM protein is present. It is not possible to distinguish between high affinity stoichiometric binding (and therefore 2 sites occupied) or binding at 1 site with lower affinity ($K_d \approx 400\ \mu$M). But, it is significant that PDC binding, as with NADH binding, does not occur at all 4 monomers. This again suggests half-the-sites (or less) activity for DHPR.

In terms of implications for fragment assembly efforts targeting DHPR, these cooperativity data also suggest the

possibility of binding selectivity and affinity differences for different monomeric sites, which could lead to selection of different fragments. Furthermore, these results provide an explanation for the occasionally observed differences between steady state inhibition (K_i) and NMR-based K_d measurements for inhibitors—the latter of which can also vary depending on whether titrations rely on ligand binding in fast exchange (ex. STD) or not (ex. HSQC), assuming some monomer sites are low and others are high affinity.

Cooperativity Model. In terms of a cooperativity model for binding substrates, our data are more consistent with the Koshland, Nemethy, and Filmer (KNF) sequential model (*21*) than with the Monod, Wyman, and Changeux (MWC) symmetry model (*22*). In the MWC model, tetrameric protein equilibrates only between two symmetric states, R and T, with the R state having higher affinity for ligand. In contrast, the KNF model permits conformational changes sequentially at each monomer, and unlike the MWC model, permits negative homotropic cooperativity. The KNF model also has the protein present in only one conformation in the absence of ligand. Our HSQC titration with NADH clearly indicates one monomeric site is occupied before the other three (Figure 6), which indicates negative cooperativity between the first and second binding events. It also indicates an asymmetric relationship between monomers, which is only permitted in the KNF sequential model. The slow exchange spectra (esp. looking at Trp253, as a reporter) in Figures 8 and 10 clearly indicate that that are two major monomer orientations (in slow exchange, with $k_{ex} < 120-270$ s^{-1}), and that ligand binding affects only the relative population of these two states. This is also true in the fast exchange spectra (Figures 7 and 9), but the fact that there are only two states is less obvious because under fast exchange conditions, crosspeak position (rather than intensity) is a population weighted average. Still, the monotonic change in chemical shift (for both ^1H and ^{15}N) during the PDC titration (Figure 7; fast exchange) is most consistent with one conformational state being converted to another, without any intermediate states. The titration of apo DHPR with NADH is also in fast exchange, but gives smaller changes (Figure 9). A plot of chemical shift changes (Figure 6) indicates the stoichiometry of binding, with 1 NADH binding to the DHPR tetramer first (i.e., with higher affinity), followed by the other NADH equivalents, but with the same chemical shift perturbation trend (as with PDC binding to apo DHPR). This leads to the NADH sequential binding model shown in Figure 1d. Whether the final tetramer is fully symmetric is not clear and whether all four sites are occupied is also not clear. What is known, simply, is that there are two NADH binding events, and the first involves binding of only 1 NADH equivalent. It is also possible that the second binding event involves only 2 NADH molecules (rather than 3), which would lead more readily to the ternary complex that has been crystallized (Figure 13).

What might be the source of the negative cooperativity between sequential NADH binding events? While a number of structural changes occur upon NADH binding, one of the most dramatic involves Arg16 movement from being directed outward toward solvent, to now flipping in to make contact with the pyrophosphate of NADH. Coupled to this change is a movement of an intermonomer contact loop containing Glu51, such that this residue changes from being 17 Å from its partner on the adjacent monomer in the open/closed pair, to now being only 5.7 Å in the closed/closed conformation pair (Figure 12d). Thus, one possible mechanism is that NADH binding interactions, which overall are favorable and mediated in part by Arg16, trigger a structural rearrangement that leads to repulsive interactions between adjacent monomers if both have NADH bound; the repulsive interaction would be mediated by Glu51 residues on adjacent monomers.

Implications for Fragment Assembly Using CRAA. Does fragment assembly and inhibitor design require one to mimic the native NADH and DHP ternary complex that forms in the steady state, or any other state of the DHPR catalytic reaction? One would speculate that this might be the case. This would mean that if the native substrates (NADH; DHP) bind synergistically, and/or with cooperativity, then fragments that occupy those binding sites (CRAA; PDC) should do the same. It should be noted that synergy refers not only to relative affinity (i.e., fragment-1 may bind tighter in the presence or absence of fragment-2), but also to structural effects. That is, fragment-1 and/or fragment-2 may induce a structural change that brings them into close proximity. This is clearly the case in DHPR, where binding of PDC induces large structural changes that bring the two binding pockets into close proximity, and may affect the extent to which ligands are buried in protein.

The fact that a high affinity biligand inhibitor of DHPR (comprised of CRAA and PDC) has already been reported, presents a unique opportunity to characterize interactions with the fragments from which it was constructed, to extract any lessons that could help in future rational biligand design projects with DHPR. The CRAA scaffold and PDC ligand are both "rigid" building blocks, occupying adjacent NADH and DHP sites, and the biligand of these two fragments shows very high affinity for DHPR ($K_i = 100$ nM), which was demonstrated in a steady state competitive inhibition study (*13*). But, CRAA and PDC do not even bind simultaneously in the studies reported herein (Figure 2). This must be an artifact of charge−charge repulsion between the two fragments when bound to DHPR, because a propylamide derivative of CRAA was reported to bind in the presence of PDC (*13*). This provides an important lesson in fragment assembly, to be cautious of screening fragments that may have repulsive interactions with other fragments that might bind at an adjacent site, and could therefore have been good candidates for biligand design. A related concern is that using competitive STD or HSQC screening in this case might have led to the false conclusion that CRAA binds in the PDC site, when in fact it binds in the adjacent NADH site.

Besides considering effects of binding synergy between adjacent-binding ligands, one should also consider effects of cooperativity. For example, PDC binds cooperatively in DHPR. If we identify alternate fragments to replace PDC, must they also bind cooperatively to inhibit enzymatic turnover, and to achieve adequate binding affinity? Unfortunately, our studies cannot address this question directly, until we identify an analog of PDC that binds without cooperativity, and see if it inhibits differently in NMR binding assays versus steady state inhibition assays. Also associated with cooperative binding is the related question as to whether one must bind at 1, 2, 3 or all 4 of the PDC sites in the tetramer. Our data indicate that only 2 of the PDC sites must be occupied, and only 1 of the NADH sites,

in order to inhibit in the steady state; therefore, all four sites in the tetramer are not equivalent. The main cautionary message here, then, is that NMR-based identification of ligands that bind to tetrameric proteins (which have non-equivalent binding sites) may or may not produce inhibitors that are relevant in the steady state, depending upon which of the nonequivalent sites they bind to preferentially. In other words, if an enzyme has half-the-sites reactivity in the steady state, ligands discovered in direct binding assays could bind in the half-that are catalytically active, in the other half, or both.

Other considerations for fragment assembly, based on our results, are that: (a) PDC might not bind as synergistically as DHP does in the steady state, suggesting a higher affinity biligand could still be designed, (b) STD_{max} and HSQC data indicate that NADH induces conformational changes needed to form the PDC binding pocket, but these are only modest changes; had they been more dramatic, one might have needed to ensure that the NADH mimic (CRAA in this case) induced the same required conformational changes, and (c) there was little binding synergy between NADH and PDC - this may have simplified the constraints on biligand assembly using substrate mimics (is it possible to design biligands, if the fragments must bind with high synergy?). (d) This potential "advantage", due to the apparent lack of binding synergy, must be viewed in the context of the fact that PDC binds with a high level of cooperativity (Hill coefficient ~2), and also induces large structural changes within a given monomer (facilitating the open => closed conformational change), meaning a successful biligand might need to be tested to verify that it can do likewise. This is a serious concern, and might explain why it was so difficult to identify other fragments that bind in the DHP substrate pocket, to permit construction of high affinity biligand inhibitors with CRAA. With hindsight, this is perhaps not surprising, since binding interactions (i.e., enthalpic contributions) with two fragments must induce structural changes that bring the fragments into close proximity for covalent linkage to be useful (i.e., without an undue entropic penalty on binding the biligand), and PDC clearly plays a significant role in inducing this domain closure. If some fragment other than PDC were used as part of the biligand, it would probably not have been as effective unless it, like PDC, could induce the structural changes needed to bring the two binding sites into proximity. Fragment assembly efforts that screen only for binding in the substrate site, without verifying that there is domain closure (Figure 12b), would not produce fragments of any utility as biligands with CRAA, since the two fragments are not in proximity of each other. As one final lesson: (e) fragment screening using either changes in STD values or in chemical shift changes (HSQC) can often be misleading in two-site enzymes, where binding at one site causes conformational changes at the other site. A prime example of this effect is the increased STD signal observed for PDC upon binding of NADH (Figure 2), or the decreased STD signal observed for NADH due to PDC binding. That is, changes in STD signal (increases or decreases) simply indicate there is binding somewhere in the protein, not necessarily that the ligands are competing for the same site.

In summary, binding synergy and cooperativity effects are clearly present in DHPR. They suggest a mechanism with half-the-sites reactivity (or less) for DHPR, and provide an explanation for differences observed between measurements of ligand affinity using different methods, especially steady state inhibition vs NMR-based titrations. DHPR binds its substrates via a KNF sequential model. In characterizing synergy effects, one must also include a consideration of structural effects transmitted between binding sites. In this regard, PDC binding causes dramatic structural changes that are transmitted to the NADH pocket, and vice-versa. Finally, a detailed characterization of synergy and cooperativity effects provides an essential foundation upon which to interpret results from NMR-guided fragment assembly efforts, which can be especially complicated in such enzyme systems.

ACKNOWLEDGMENT

We thank Dr. John Blanchard (Albert Einstein College of Medicine, New York) for the DHPR (dapB) and DHPS (dapA) expression constructs. We also thank the Nathan Hale SMART team and Milwaukee School of Engineering for building a protein model of DHPR, as part of an NIH-NCRR-SEPA funded outreach program (R25-RR022749); this model was an essential tool in helping to visualize and understand intermonomer interactions.

SUPPORTING INFORMATION AVAILABLE

Gels, HSQC spectra, titration curves, and fitting results. This material is available free of charge via the Internet at http://pubs.acs.org.

REFERENCES

1. Pavelka, M. S., Jr., and Jacobs, W. R., Jr. (1996) Biosynthesis of Diaminopimelate, the Precursor of Lysine and a Component of Peptidoglycan, Is an Essential Function of *Mycobacterium smegmatis*. *J. Bacteriol. 178*, 6496–6507.
2. Paiva, A. M., Vanderwall, D. E., Blanchard, J. S., Kozarich, J. W., Williamson, J. M., and Kelly, T. M. (2001) Inhibitors of Dihydrodipicolinate Reductase, a Key Enzyme of the Diaminopimelate Pathway of *Mycobacterium Tuberculosis*. *Biochim. Biophys. Acta 1545*, 67–77.
3. Scapin, G., Blanchard, J. S., and Sacchettini, J. C. (1995) Three-Dimensional Structure of *Escherichia coli* Dihydrodipicolinate Reductase. *Biochemistry 34*, 3502–3512.
4. Scapin, G., Reddy, S. G., Zheng, R., and Blanchard, J. S. (1997) Three-Dimensional Structure of *Escherichia coli* Dihydrodipicolinate Reductase in Complex with NADH and the Inhibitor 2,6-Pyridinedicarboxylate. *Biochemistry. 36*, 15081–15088.
5. Cirilli, M., Zheng, R., Scapin, G., and Blanchard, J. S. (2003) The Three-Dimensional Structures of the *Mycobacterium tuberculosis* Dihydrodipicolinate Reductase-NADH-2,6-PDC and -NADPH-2,6-PDC Complexes. Structural and Mutagenic Analysis of Relaxed Nucleotide Specificity. *Biochemistry 42*, 10644–10650.
6. Reddy, S. G., Scapin, G., and Blanchard, J. S. (1996) Interaction of Pyridine Nucleotide Substrates with Escherichia Coli Dihydrodipicolinate Reductase: Thermodynamic and Structural Analysis of Binary Complexes. *Biochemistry 35*, 13294–13302.
7. Kefala, G., and Weiss, M. S. (2006) Cloning, Expression, Purification, Crystallization and Preliminary X-Ray Diffraction Analysis of DapA (Rv2753c) from *Mycobacterium tuberculosis*. *Acta Crystallograph Sect. F. Struct. Biol. Cryst. Commun. 62*, 1116–1119.
8. Hajduk, P. J., and Greer, J. (2007) A Decade of Fragment-Based Drug Design: Strategic Advances and Lessons Learned. *Nat. Rev. Drug Discovery 6*, 211–219.
9. Alex, A. A., and Flocco, M. M. (2007) Fragment-Based Drug Discovery: What has it Achieved so Far? *Curr. Top. Med. Chem. 7*, 1544–1567.
10. Leach, A. R., Hann, M. M., Burrows, J. N., and Griffen, E. J. (2006) Fragment Screening: An Introduction. *Mol. Biosyst. 2*, 430–446.

11. Carr, R. A., Congreve, M., Murray, C. W., and Rees, D. C. (2005) Fragment-Based Lead Discovery: Leads by Design. *Drug Discovery Today 10*, 987–992.
12. Hajduk, P. J. (2006) Puzzling through Fragment-Based Drug Design. *Nat. Chem. Biol. 2*, 658–659.
13. Sem, D. S., Bertolaet, B., Baker, B., Chang, E., Costache, A. D., Coutts, S., Dong, Q., Hansen, M., Hong, V., Huang, X., Jack, R. M., Kho, R., Lang, H., Ma, C. T., Meininger, D., Pellecchia, M., Pierre, F., Villar, H., and Yu, L. (2004) Systems-Based Design of Bi-Ligand Inhibitors of Oxidoreductases: Filling the Chemical Proteomic Toolbox. *Chem. Biol. 11*, 185–194.
14. Ge, X., and Sem, D. S. (2007) Affinity-Based Chemical Proteomic Probe for Dehydrogenases: Fluorescence and Visible Binding Assays in Gels. *Anal. Biochem. 370*, 171–179.
15. Salzmann, M., Pervushin, K., Wider, G., Senn, H., and Wuthrich, K. (1998) TROSY in Triple-Resonance Experiments: New Perspectives for Sequential NMR Assignment of Large Proteins. *Proc. Natl. Acad. Sci. U. S. A. 95*, 13585–13590.
16. Sem, D. S., and Pellecchia, M. (2001) NMR in the Acceleration of Drug Discovery. *Curr. Opin. Drug Discovery Devel. 4*, 479–492.
17. Pellecchia, M., Sem, D. S., and Wuthrich, K. (2002) NMR in Drug Discovery. *Nat. Rev. Drug Discovery 1*, 211–219.
18. Mayer, M., and Meyer, B. (2001) Group Epitope Mapping by Saturation Transfer Difference NMR to Identify Segments of a Ligand in Direct Contact with a Protein Receptor. *J. Am. Chem. Soc. 123*, 6108–6117.
19. Colowick, S. P., Kaplan, N. O., and Ciotti, M. M. (1951) The Reaction of Pyridine Nucleotide with Cyanide and its Analytical Use. *J. Biol. Chem. 191*, 447–459.
20. Reddy, S. G., Sacchettini, J. C., and Blanchard, J. S. (1995) Expression, Purification, and Characterization of. *Escherichia coli Dihydrodipicolinate Reductase. Biochemistry 34*, 3492–3501.
21. Koshland, D. E., Jr, Nemethy, G., and Filmer, D. (1966) Comparison of Experimental Binding Data and Theoretical Models in Proteins Containing Subunits. *Biochemistry 5*, 365–385.
22. Monod, J., Wyman, J., and Changeux, J. P. (1965) On the Nature of Allosteric Transitions: A Plausible Model. *J. Mol. Biol. 12*, 88–118.

BI8007005